Facile Ultrasonic Synthesis of CoO Quantum Dot/Graphene Nanosheet Composites with High Lithium Storage Capacity

Chengxin Peng,[†,⊥] Bingdi Chen,[†,⊥] Yao Qin,[†] Shihe Yang,[‡] Chunzhong Li,[§] Yuanhui Zuo,[†] Siyang Liu,[†] and Jinhu Yang[†,*]

[†]Institute for Advanced Materials & Nano Biomedicine and Department of Chemistry, Tongji University, Chifeng Road 67, Shanghai 200092, China, [‡]Nano Science and Technology Program, Department of Chemistry, William Mong Institute of Nano Science and Technology, The Hong Kong University of Science and Technology, Clear Water Bay, Kowloon, Hong Kong, China, and [§]Key Laboratory for Ultrafine Materials of Ministry of Education, School of Materials Science and Engineering, East China University of Science and Technology, Shanghai 200237, China. [⊥]These authors contributed equally to this work.

ABSTRACT In this paper, we report a facile ultrasonic method to synthesize well-dispersed CoO quantum dots (3−8 nm) on graphene nanosheets at room temperature by employing $Co_4(CO)_{12}$ as cobalt precursor. The prepared CoO/graphene composites displayed high performance as an anode material for lithium-ion battery, such as high reversible lithium storage capacity (1592 mAh g^{-1} after 50 cycles), high Coulombic efficiency (over 95%), excellent cycling stability, and high rate capability (1008 mAh g^{-1} with a total retention of 77.6% after 50 cycles at a current density of 1000 mA g^{-1}, dramatically increased from the initial 50 mA g^{-1}). The extraordinary performance arises from the structure advantages of the composites: the nanosized CoO quantum dots with high dispersity on conductive graphene substrates supply not only large quantity of accessible active sites for lithium-ion insertion but also good conductivity and short diffusion length for lithium ions, which are beneficial for high capacity and rate capability. Meanwhile, the isolated CoO quantum dots anchored tightly on the graphene nanosheets can effectively circumvent the volume expansion/contraction associated with lithium insertion/extraction during discharge/charge processes, which is good for high capacity as well as cycling stability. Moreover, regarding the anomalous behavior of capacity increase with cycles (activation effect) observed, we proposed a tentative hypothesis stressing the competition between the conductivity increase and the amorphorization of the composite electrodes during cycling in determining the trends of the capacity, in the hope to gain a fuller understanding of the inner working of the novel nanostructured electrode-based lithium-ion batteries.

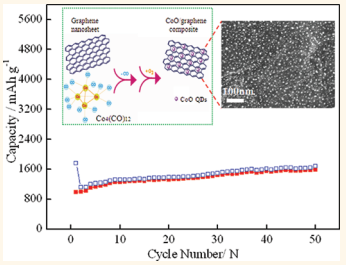

KEYWORDS: ultrasonic synthesis · CoO quantum dots · graphene · composites · lithium-ion batteries · anode materials · lithium storage capacity

Rechargeable lithium-ion batteries (LIBs) are the leading power sources for portable electronic devices and electrical/hybrid vehicles owing to their high energy density, light weight, and long service life.[1−3] Electrode materials wherein are important components in determining LIB's performance. However, commercial graphite anodes used currently have a low gravimetric capacity of 372 mAh g^{-1}, which leads to a limited energy output of LIBs.[4] To meet ever-increasing demand for LIBs with high energy density, transition metal oxides (MO_X, M: Fe, Co, Ni, Cu, *etc.*), an alternative group of promising candidates with high theoretical capacities (>600 mAh g^{-1}), have been exploited as anode materials for high-performance LIBs since the 1980s.[5−7] Among these MO_X, cobalt monoxide (CoO) has attracted special attention due to its higher theoretical Li-ion storage capacities (716 mAh g^{-1}) and, moreover, its completely reversible electrochemical reaction ($CoO + 2Li^+ + 2e \rightleftharpoons Co + Li_2O$).[8−12]

However, the MO_X materials have poor conductivity and suffer from large volume expansion/contraction associated with Li^+-ion insertion/extraction during the discharge/charge processes, which may lead to an irreversible capacity loss and poor cycling stability.[13,14] To circumvent these problems, graphitic carbons such as graphite[15] and carbon nanofiber[16]/nanotube[17] often serve as conductive matrices to load MO_X for improved performance. Particularly, graphene, a two-dimensional (2D) carbon atom monolayer, is recently becoming one of the most appearing matrices for metal oxides due to its unique properties, such as superior electric conductivity, high surface area over 2600 m^2 g^{-1}, excellent mechanical flexibility, as well as a high theoretical lithium storage of 744 mAh g^{-1}.[18−21] The addressing of graphene could both increase conductivity and surface area of the electrodes and buffer the strain from the volume change of metal oxides during discharge/charge processes. By far, a

* Address correspondence to yangjinhu2010@gmail.com.

Received for review July 30, 2011 and accepted January 8, 2012.

Published online January 09, 2012
10.1021/nn202888d

number of hybrid materials consisting of graphene and metal oxides, such as Fe_3O_4/Fe_2O_3,[22−26] Co_3O_4/CoO,[27−31] Mn_3O_4,[32] NiO,[33] CuO/Cu_2O,[34,35] SnO_2,[36−38] and TiO_2,[39−41] have been prepared as anode materials for LIBs.

It is noteworthy, on the other hand, that the size and dispersion of metal oxides on graphene are crucial factors for improving cell performance[42−44] because small particle size plus good dispersion (*e.g.*, down to several nanometers) can endow the composite electrode a superior high surface area to buffer the volume change of the oxides, but it could also bring the required conductivity to individual nanoparticles and shorten the diffusion length for Li^+ ions, which are beneficial for high lithium storage and rate capability,[42] respectively. According to literature, however, most metal oxide/graphene composites prepared so far have relatively bigger MO_X sizes (over 10 nm up to hundreds of nanometers) with unsatisfying dispersions. Furthermore, the main routes[22−27,29−36,38−41] commonly used for the preparation of the metal oxide/graphene composites were either carried out with complicated processes or suffered often from poor manipulation on metal oxide/graphene. Therefore, it is highly desired to develop a facile and general approach for the synthesis of MO_X/graphene composites with favored structures for high-performance LIBs.

In this paper, we design a facile one-step ultrasonic way to synthesize CoO quantum dots (3−8 nm) (QDs) on graphene nanosheets (GNs) by using a metal carbonyl ($Co_4(CO)_{12}$) cluster as the precursor at ambient temperature (see Scheme 1). The ultrasonic reaction involves a two-step reaction mechanism: metallic Co generation on GNs from $Co_4(CO)_{12}$ precursor decomposition under sonication (step I) and, subsequently, followed by Co oxidization *in situ* into CoO by solution-dissolved O_2 (step II). The strong interaction between electron-rich Co atoms and electrophilic carbon atoms of graphene allows Co and CoO QDs to be tightly anchored on graphene matrices before and after oxidization. Meanwhile, ultrasonic condition enables graphene to accommodate CoO QDs at maximum with an unstacked active surface. Such composites with the well-dispersed CoO QDs anchored firmly on the GNs are advantageous for inhibiting aggregation and volume change of MO_X during cycling and offer a direct short pathway for Li^+ diffusion. As expected, as an anode material for LIBs, the typical CoO quantun dot/graphene nanosheet (CQD/GN) composites exhibited very high reversible lithium storage capacity and excellent rate capability.

RESULTS AND DISCUSSION

GNs (see characterizations in Figure S1 of the Supporting Information) were used as highly effective

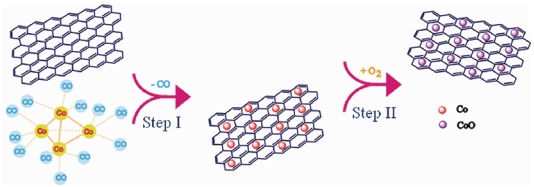

Scheme 1. Schematic illustration for the *in situ* formation mechanism of the CoO/graphene composites.

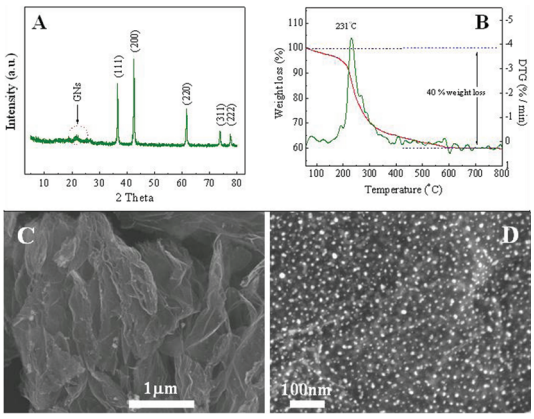

Figure 1. (A) XRD pattern, (B) TGA, and (C,D) SEM images of the CQD/GN composites.

matrices for the preparation of the typical CQD/GN composites. The XRD pattern of the nanocomposites in Figure 1A displays sharp peaks corresponding to the face-centered cubic (fcc) structure of cobalt monooxide (CoO, JCPDS 48-1719) and a weak broadened peak at 22−28°, which can be ascribed to the {200} plane refractions of graphene,[45] indicating the composites are made of well-crystallized CoO and graphene. The TGA measurement in Figure 1B further determines a mass ratio of 60:40 (CoO/graphene) of the two materials in the composites. The morphology of the nanocomposites was primarily studied by SEM. The low-magnification image in Figure 1C presents a curved shape of the nanosheets with a looser stacking style, compared with pure graphene before CoO loading (see Figure S1). This implies that the CoO existence is helpful for the separation of the GNs. A high-magnification SEM image (Figure 1D) shows that the CoO QDs hold small sizes less than 10 nm (3−8 nm) and are uniformly distributed on the GNs.

More close observations by TEM on morphology and structure of the CQD/GN composites are given in Figure 2. A low-resolution TEM image (Figure 2A) of an individual composited nanosheet exhibits a curved characteristic and a low contrast, revealing an ultrathin thickness of the nanosheets with CoO QD loading. Moreover, it can be seen that the sizes of the CoO QDs are in the range of 3−8 nm (Figure 2B,C), which is in good agreement with SEM observations above. The dispersion of the CoO QDs on GNs is very uniform but seems to be in a much denser manner (Figure 2B) in

contrast with that shown in Figure 1D. In fact, this is just visual matter caused by the TEM method. Unlike in the SEM, CoO QDs on both sides of GNs can be seen by TEM, and thus their contributions are doubled, resulting in the high density of the CoO QDs as observed. The selected area electronic diffraction pattern (inset in Figure 2C) corresponding to CoO QDs circled gives a set of diffraction rings, which can be clearly assigned to the diffractions of the {111}, {200}, and {220} planes, respectively, of the face-centered cubic structure of CoO. This result is consistent with the XRD characterization where the refractions of these planes are intensified. In addition, the high-resolution TEM image of an individual CoO QD displays clear crystal lattice with a spacing of 0.22 nm corresponding to the (220) plane. Therefore, from the structural analyses, it is certain that the QDs distributed uniformly on the graphene are pure CoO and well-crystallized.

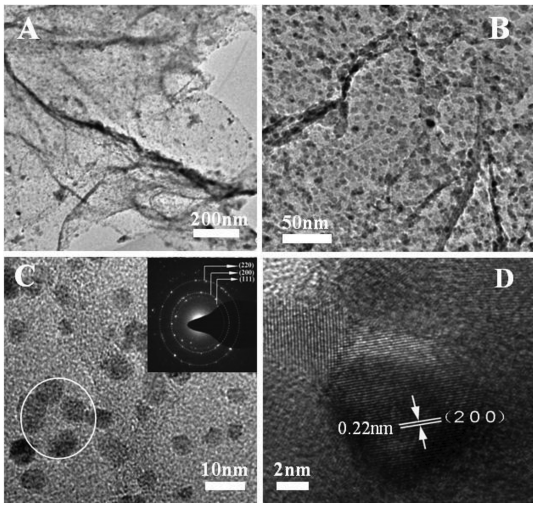

Figure 2. (A–C) TEM images and (D) high-resolution TEM image of the CQD/GN composites. Inset in C is the electronic diffraction pattern corresponding to the CoO QDs circled.

We think the rational selection of the $Co_4(CO)_{12}$ precursor and the ultrasonic method is critical for the successful preparation of the uniformly dispersed CoO QDs on graphene substrates. First, $Co_4(CO)_{12}$, as one of metal carbonyls, is easy to dissolve or disperse in/on suitable solvents/supports and can decompose readily into Co atom clusters under sonication conditions ($Co_4(CO)_{12} \rightarrow 4Co + 12CO$). This is an essential way to get the highly dispersed Co clusters on GNs and, subsequently, CoO QDs *via in situ* oxidation ($2Co + O_2 \rightarrow 2CoO$). On the other hand, the ultrasonic method provides a necessary drive for the complete decomposition of $Co_4(CO)_{12}$ and also for avoiding aggregation of the as-produced Co/CoO and restacking of the GNs, which ensures an efficient way for the graphene support to load the Co clusters or CoO QDs with large and active surfaces. Of course, the electrostatic attraction between electron-rich Co atoms and electron-unsaturated carbon atoms of graphene can enable Co or CoO to be firmly anchored on the graphene surface and thus enhance the conjunction stability of the hybrids.

Figure 3 shows the electrochemical performance of the typical CQD/GN composites. As shown in Figure 3A,

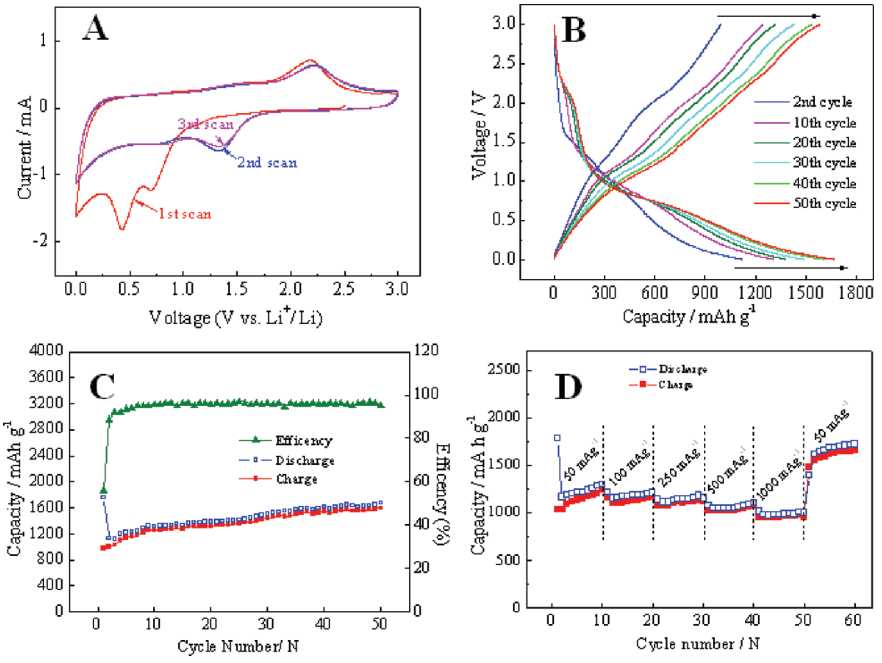

Figure 3. (A) Cyclic voltammograms of the CQD/GN composites in a voltage range of 0.0–3.0 V at a scanning rate of 1 mV s^{-1}. (B) Galvanostatic charge–discharge curves cycled at the 2nd, 10th, 20th, 30th, 40th, and 50th cycle of the CQD/GN composites between 3.00 and 0.01 V at a current density of 50 mA g^{-1}. (C) Cycling performance and (D) rate capability of the CQD/GN composites at the current densities between 50 and 1000 mA g^{-1}.

a cyclic voltammogram (CV) test was applied to investigate the detailed electrochemical properties at a scan rate of 1 mV/s within the voltage window of 0.01−3.00 V. Two cathodic peaks at voltage potentials of 0.7 and 0.43 V are observed in the first cathodic scan, while they disappeared in the following scans, which is due to the irreversible formation of a solid electrolyte interphase (SEI) and the decomposition of electrolyte.[46,47] In subsequent cycles, the cathodic peaks shift to 1.3 V and tends to be stable. In the anodic scans, the peaks at 2.2 V are recorded. These cathodic and anodic peaks at 1.3 and 2.2 V correspond to the electrochemical reduction/oxidation (CoO ⇌ Co) reactions accompanying Li^+ insertion (lithiation) and extraction (delithiation).[15] In addition, the sharp reduction peak at 0.02 V and the broad oxidation peak at 0.27 V are ascribed to the insertion/extraction of Li into/from graphene,[27] suggesting that the graphene in the composites is also electroactive for lithium storage.

Figure 3B presents the charge/discharge profiles of the CQD/GN composites in the 2nd, 10th, 20th, 30th, 40th, and 50th cycles at a current density of 50 mA g^{-1}. In accordance with the CV analysis above, three voltage plateaus are observed during the charge/discharge processes. The presence of a sloping discharge plateau at 1.5−0.7 V corresponds to the generation of Li_2O accompanying the reduction of CoO into metal Co. The occurrence of two sloping plateaus at *ca.* 1.2 and 2.2 V in the charge processes should be ascribed to the oxidation reaction of Co with Li_2O.[11] The following sloping curves go down to the cutoff voltage of 0.01 V, which indicates the insertion/extraction of lithium to graphene.[48] The discharge plateau shifts gradually to a low potential range of 1.2−0.7 V upon cycling, implying that the discharge process involving homogeneous distribution of amorphous Co embedded in the Li_2O matrix has been built.[42] Thus a high reversible capacity and excellent cycling performance can be achieved. As illustrated in Figure 3B, we can see that the CQD/GN composites display increasing high capacities with cycles from 1120 mAh g^{-1} in the second cycle to 1690 mAh g^{-1} in the 50th cycle. This trend recurs in the cycle performance test, as shown in Figure 3C.

Figure 3C shows the cycling performance of the CQD/GN composites at a current density of 50 mA g^{-1}. It can be seen that the sample delivers a superhigh lithium storage capacity of about 1756 mAh g^{-1} during the first discharge process. However, a relative low charge capacity of 980 mAh g^{-1} is achieved, corresponding to a Coulombic efficiency of 56%. The large irreversible capacity loss during the first discharge/charge process is mainly related to the irreversible lithium loss due to the SEI layer formation. This characteristic agrees well with the CV result that the cathodic peaks are present in the first scan while absent afterward. In the second cycle, the Coulombic efficiency increases to 95% and a discharge capacity of 996.2 mAh g^{-1} is achieved, which is much higher than the theoretical value for CoO/graphene composites ($C_{theoretical} = C_{CoO} \times$ mass percentage of CoO + $C_{graphene} \times$ mass percentage of graphene = 716 × 60% + 744 × 40% = 727.2 mAh g^{-1}). It is reported that the graphene nanosheets have significant disorder/defects, which can also contribute to the lithium storage capacity,[49] in addition to the intrinsic theoretical capacity (formation of intercalation compounds Li_3C[50]). Besides, the reversible decomposition of the electrolyte with the formation of SEI and extra lithium-ion adsorption/desorption on the SEI while cycling may lead to the high experimental lithium storage capacity, as well.[8,47] More interestingly, the reversible capacities show an upward trend with the cycles, similar to that in galvanostatic charge/discharge analysis (Figure 3B), from the second cycle up to the 50th cycle. After 50 cycles, the reversible capacity of the CQD/GN composites reaches 1592 mAh g^{-1}, demonstrating the high lithium storage capability and the excellent cycling behavior of the sample. To the best of our knowledge, this is the highest reported capacity for cobalt-oxide-based LIB anode materials.

In addition, the CQD/GN composites exhibited excellent rate capability. As shown in Figure 3D, the CQD/GN composites show a reversible capacity as high as 1299 mAh g^{-1} after the 10th cycle at a current density of 50 mA g^{-1}, then 1206 mAh g^{-1} after the 20th cycle at 100 mA g^{-1}, 1177 mAh g^{-1} after the 30th cycle at 250 mA g^{-1}, 1100 mAh g^{-1} after the 40th cycle at 500 mA g^{-1}, and 1008 mAh g^{-1} after the 50th cycle at 1000 mA g^{-1}. The excellent retention in total of 77.6% is obtained when the current density is enlarged 20 times from 50 to 1000 mA g^{-1}. Moreover, when the rate returns from 1000 mA g^{-1} to the initial 50 mA g^{-1}, the composite electrode releases a much higher reversible capacity (1719 mAh g^{-1}) after the 60th cycle than the initial one. It can be detected that, in spite of high current densities applied, the increasing slope (capacity *versus* cycle) in rate capability is approximately comparable to that in cycling performance conducted at the same 50 mA g^{-1} (Figure 3C), indicating the extraordinarily high cycling stability. Furthermore, the rate capability of the typical CQD/GN composites performed in another wider current density range from 50 to as high as 4000 mA g^{-1} also displays high cycling stability and good retention, as listed in Figure S2. The extraordinary performance relies on the specific structure of the sample that offers the good conductivity of the electrode for fast Li^+-ion diffusion, the large quantity of accessible sites for Li^+ insertion, and the nanoscaled uniform dispersity for improved reversibility of reactions.

Influence of synthesis parameters, including $Co_4(CO)_{12}$ concentration and sonication, on CQD/GN composite structures and their lithium-ion performance

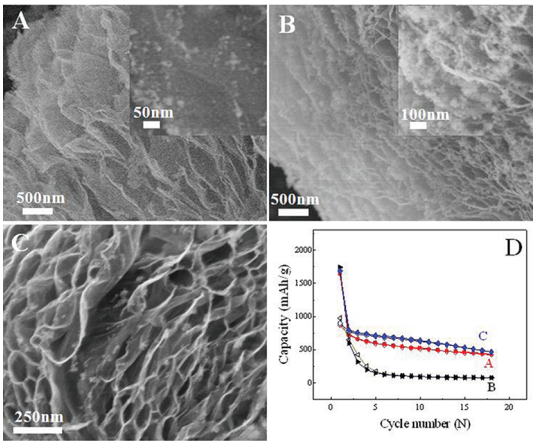

Figure 4. SEM images (A−C) of CoO/graphene nanocomposites at different synthesis conditions and their cycling performance (D) at a high current density of 1000 mA g^{-1}. The synthesis conditions were kept typical except half (A) and double (B) $Co_4(CO)_{12}$ precursor concentration and stirring instead of sonication (C) were applied.

has been investigated, as well, as shown in Figure 4. Relatively lower CoO load (Figure 4A) and much higher CoO load with severe aggregation (Figure 4B) on the graphene nanosheets were obtained at half and double $Co_4(CO)_{12}$ precursor concentration, while analogous CoO load with slight aggregation was produced at the same $Co_4(CO)_{12}$ concentration with stirring instead of sonication, respectively, compared with that of the typical CQD/GN composites. The cycling performance of these samples at a high current density of 1000 mA is shown in Figure 4D. It can be seen that capacities of all three samples start from around 900 mAh g^{-1} at the first cycle and then decrease upon cycling. In contrast, their performances are apparently worse than that of the typical CQD/GN sample at the same current density of 1000 mA g^{-1} after tens of cycles (Figure 3D and Figure S2), where both higher capacity over 1000 mAh g^{-1} and stable capacity behavior were achieved. It can be analyzed that the low capacity of samples A and C should mainly result from less CoO loading and poor CoO dispersion, which respectively lead to less active sites and poor Li^+-ion diffusion, whereas the rapid capacity decay of sample B is probably ascribed to the severe aggregation due to CoO overloading, which will cause poor conductivity and even electrode pulverization with cycles.

It should be noted that, usually, LIB capacity fades with cycles, regardless of rates. This is normally caused by the deactivation of oxides or the disability of lithium insertion/extraction during long-time cycling. In previous reports, the anomalous behaviors of capacity increase upon cycling were discovered and rationally attributed to the reversible growth of pseudocapacitive polymeric film.[51] However, since LIBs are quite complex systems, there is probably more than one factor associated with this phenomenon, which motivates us to probe the mechanism fuller. As mentioned in the preparation section, the amorphous CoO was prepared on the GNs before heat treatment (Figure S3A−C). Compared with the thermally treated crystallized CoO QDs, the amorphous CoO has otherwise no difference except higher dispersity (isolated small grains at atomic scale) and consequentially poorer conductivity. It can be deduced that the higher dispersity offering more accessible active sites for lithium insertion could give rise to a higher lithium storage capacity, while the poorer conductivity exerts an opposite effect by hindering Li^+-ion diffusion and insertion ($CoO + 2Li^+ + 2e \rightarrow Co + Li_2O$), leading to the capacity fading. To our surprise, the analysis is validated experimentally: the amorphous CoO/graphene composites deliver a superhigh lithium storage capacity of 2000 mAh g^{-1} in the first discharge process (see Figure S3D, the cycling performance at a current density of 50 mA g^{-1}), which is much higher than that of the crystallized CQD/GN composites (1756 mAh g^{-1}). Nevertheless, the capacity fades constantly to 700 mAh g^{-1} after 50 cycles due to poor conductivity. The above experimental facts give us a valuable indication to explain the anomalous capacity increase tentatively: (i) during the cycling processes, with reversible lithium insertion/extraction, the crystallized MO_X changed gradually to be amorphous, which had been well researched,[16] as also confirmed by the XRD result of the CQD/GN composites after cycling processes (Figure S4). This means, in other words, that more and more accessible active sites were available for Li^+-ion insertion, expressing definitely as the constant growth of capacity; (ii) on the other hand, the conductivity of the MO_X/graphene electrode decreases during the cycling, correspondingly, leading to the capacity decrease. Obviously, the two factors play a competitive role in determining the trends of capacity. In detail, for (i) dominated processes, the capacities increase with cycles (so-called activation processes), which is adaptable to our case that the continual capacity increase of the CQD/GN composites during all 50 cycles (see Figure S5, type 1); while for (ii) dominated processes, the capacity goes down oppositely—this is common behavior for most MO_X-based LIBs (see Figure S5, type 2); when (i) and (ii) reach an equilibrium at a point during the cycling, the maximum capacity could be achieved (Figure S5, type 3), corresponding to some cases observed in previous reports.[8,10,16,22] It can be further predicted that if more cycles are applied in the cycling performance for our crystallized CQD/GN composites, the capacity will reach a maximum and then drop, due to the steeply decreasing the conductivity upon later cycling. To verify this prediction, more cycles following cycling performance measurement of Figure 3C were applied to the typical CQD/GN composites. It was found that the capacity still increases with cycles until the 69th cycle and then decreases gradually (Figure S6), which confirms our proposed

hypothesis. So, strictly, type 1 should be the early half part of the type 3, and the presence of the type 1 (or activation processes) is dependent, to some extent, on the structure of the composite electrodes, such as shape, size, as well as dispersity of MO_X. We think the size down to several nanometers, good dispersity of MO_X, and the compact contact of MO_X/supports are favorable for such activation processes. We hope that our explanation could be helpful for better understanding the correlation between MO_X-based electrodes and LIB performance during the discharge/charge processes.

CONCLUSION

In summary, we have presented a novel ultrasonic approach for the facile synthesis of the CQD/GN composites by choosing $(Co)_4CO_{12}$ as the precursor. The CoO QDs held an average diameter of ~5 nm and uniform dispersity on the GNs. Such CoO/graphene hybrid architecture is ideal for lithium storage. First, the CoO QDs in small size with the high mass load (60%) provided a great deal of active sites, which was responsible for the high lithium capacity. Meanwhile, the CoO QDs that firmly anchored on the GNs could avoid serious volume change and agglomeration of the oxides caused by lithium insertion/extraction, thereby ensuring a high reversibility during the discharge/charge processes, which accounted for the high cycling stability. Moreover, the isolated nanosized CoO on the conductive graphene support could not only endow each CoO QD with the required conductivity but also give the diffusion shortcut for Li^+ ions. This would significantly facilitate the lithium diffusion kinetics and lead to the excellent rate capability. As a result, the CQD/GN hybrid electrode demonstrated extraordinary performance, such as high reversible lithium storage capacity (1592 mAh g^{-1} in the 50th cycle), excellent cycling performance, and rate capability (1008 mAh g^{-1} when the discharge current enlarged 20 times to 1000 mA g^{-1}). In addition, regarding the open question that the capacity increases anomalously during the discharge/charge processes, we have analyzed on the basis of the obtained experimental results and proposed a plausible hypothesis to explain the formation mechanisms for the three types of capacity behaviors observed so far, trying to bring a fuller and clearer understanding. Besides LIBs, the CQD/GN composites with good conductivity and high dispersity are promising in other areas such as gas sensors, electro-/photocatalysis, *etc*. Furthermore, it is highly possible that this facile ultrasonic method can be extended as a general approach to other transition metal systems for the preparation of highly dispersed nanosized MO_X on graphene, by rationally choosing metal carbonyl counterparts.

METHODS

Preparation of CQD/GN Composites. The CQD/GN composites were prepared by a facile ultrasonic method at room temperature. In a typical synthesis, 40 mg of GNs (prepared *via* a modified Hummer's method[52]) was dispersed in 90 mL of hexane under sonication for 1 h, then an appropriate amount of $Co_4(CO)_{12}$ (Alfa Aesar, China) was added directly into the above solution and sonicated for another 1 h. Subsequently, the resulting products were collected by centrifugation, washed with deionized water and ethanol, and dried at 60 °C in air. The products were characterized to be amorphous CoO on the GNs at this step. Finally, the crystalline CQD/GN composites were obtained *via* a thermal treatment at 550 °C for 3 h under N_2 atmosphere.

Material Characterizations. Scanning electron microscopy (SEM, JEOL, JSM-6700F and Hitachi, S-4800), transmission electron microscopy (TEM, Philips, FEI TecnaiG 2F20), power X-ray diffraction (XRD, D/max rB, Cu Kα radiation), thermogravimetric analysis (TGA, Netzsch STA409C, measured from 30 to 900 °C at a heating rate of 10 °C/min in air), X-ray photoelectron spectra (XPS, recorded on a PHI quantera SXM spectrometer with an Al Kα = 280.00 eV excitation source; the binding energies were calibrated by referencing the C1s peak (284.6 eV) to reduce the sample charge effect), and Raman measurements (a WiTec Alpha300 system with a 532 nm wavelength incident laser light) were applied to characterize the obtained samples.

Electrochemical Measurements. Electrochemical performance was evaluated *via* CR2016-type coin cell on a LAND battery test system (CT2001A, China). The working electrode was composed of 80 wt % active material (CQD/GN composites), 12 wt % acetylene black (Super-P), and 8 wt % poly(vinylidene fluoride) (PVDF) binder dissolved in *N*-methyl-2-pyrrolidinone (NMP). Lithium foil was used as the counter and reference electrode, and polypropylene (PP) membrane (Celgard 2400) was employed as a separator. The electrolytes were 1 M $LiPF_6$ dissolved in a mixture of ethylene (EC) and diethyl carbonate (DEC) (1:1, v/v). Cyclic voltammetry (CV) measurement was carried out using Autolab 302n electrochemical workstation at a scanning rate of 1 mV s^{-1}. The batteries were assembled in an argon-filled glovebox and galvanostatic charged/discharged at various current densities of 50−1000 mA g^{-1} in the fixed voltage range of 3−0.01 V at room temperature.

Acknowledgment. We thank the National Natural Science Foundation (21001082, 20925621), Shanghai Pujiang Program (10PJ1410400), Research Fund for the Doctoral Program of Higher Education of China (20090072120013), Visiting scholar fund of the Key Laboratory for Ultrafine Materials of Ministry of Education, East China University of Science, and Technology and the Program for Young Excellent Talents in Tongji University (2008KJ046 and 2009KJ075) for financial support.

Supporting Information Available: SEM images, XRD pattern, Raman spectrum of GNs, XPS spectra, TEM image, cycling performance of the amorphous CoO/graphene composites, XRD data after cycling, the cycling and rate performance of the CQD/GN composites, and schematic diagram of capacity behaviors for MO_X-based electrodes. This material is available free of charge *via* the Internet at http://pubs.acs.org.

REFERENCES AND NOTES

1. Winter, M.; Besenhard, J. O.; Spahr, M. E.; Novak, P. Insertion Electrode Materials for Rechargeable Lithium Batteries. *Adv. Mater.* **1998**, *10*, 725–763.
2. Liu, C.; Li, F.; Ma, L. P.; Cheng, H. M. Advanced Materials for Energy Storage. *Adv. Mater.* **2010**, *22*, 28–62.
3. Guo, Y. G.; Hu, J. S.; Wan, L. J. Nanostructured Materials for Electrochemical Energy Conversion and Storage Devices. *Adv. Mater.* **2008**, *20*, 2878–2887.

4. Tarascon, J. M.; Armand, M. Issues and Challenges Facing Rechargeable Lithium Batteries. *Nature* **2001**, *414*, 359–367.
5. Thackeray, M. M.; Coetzer, J. A Preliminary Investigation of the Electrochemical Performance of α-Fe_2O_3 and Fe_3O_4 Cathodes in High-Temperature Cells. *Mater. Res. Bull.* **1981**, *16*, 591–597.
6. Thackeray, M. M.; Backer, S. D.; Adendorff, K. T.; Goodenough, J. B. Lithium Insertion into Co_3O_4: A Preliminary Investigation. *Solid State Ionics* **1985**, *17*, 175–182.
7. Thackeray, M. M.; David, W. I. F.; Bruce, P. G.; Goodenough, J. B. Lithium Insertion into Manganese Spinels. *Mater. Res. Bull.* **1983**, *18*, 461–472.
8. Poizot, P.; Laruelle, S.; Grugeon, S.; Dupont, L.; Tarascon, J.-M. Nano-Sized Transition-Metal Oxides as Negative-Electrode Materials for Lithium-Ion Batteries. *Nature* **2000**, *407*, 496–499.
9. Aricò, A. S.; Bruce, P.; Scrosati, B.; Tarascon, J.-M.; Schalkwijk, W. V. Nanostructured Materials for Advanced Energy Conversion and Storage Devices. *Nat. Mater.* **2005**, *4*, 366–377.
10. Do, J.-S.; Weng, C.-H. Preparation and Characterization of CoO Used as Anodic Material of Lithium Battery. *J. Power Sources* **2005**, *146*, 482–486.
11. Chen, C. H.; Hwang, B. J.; Do, J. S.; Weng, J. H.; Venkateswarlu, M.; Cheng, M. Y.; Santhanam, R.; Ragavendran, K.; Lee, J. F.; Chen, J. M.; *et al.* An Understanding of Anomalous Capacity of Nano-Sized CoO Anode Materials for Advanced Li-Ion Battery. *Electrochem. Commun.* **2010**, *12*, 496–498.
12. Jiang, J.; Liu, J. P.; Ding, R. M.; Ji, X. X.; Hu, Y. Y.; Li, X.; Hu, A. Z.; Wu, D.; Zhu, Z. H.; Huang, X. T. Direct Synthesis of CoO Porous Nanowire Arrays on Ti Substrate and Their Application as Lithium-Ion Battery Electrodes. *J. Phys. Chem. C* **2010**, *114*, 929–932.
13. Li, Y. G.; Tan, B.; Wu, Y. Y. Mesoporous Co_3O_4 Nanowire Arrays for Lithium Ion Batteries with High Capacity and Rate Capability. *Nano Lett.* **2008**, *8*, 265–270.
14. Yao, W. L.; Wang, J. L.; Yang, J.; Du, G. D. Novel Carbon Nanofiber–Cobalt Oxide Composites for Lithium Storage with Large Capacity and High Reversibility. *J. Power Sources* **2008**, *176*, 369–372.
15. Li, F.; Zou, Q. Q.; Xia, Y. Y. CoO-Loaded Graphitable Carbon Hollow Spheres as Anode Materials for Lithium-Ion Battery. *J. Power Sources* **2008**, *177*, 546–552.
16. Yao, W. L.; Yang, J.; Wang, J. L.; Tao, L. Synthesis and Electrochemical Performance of Carbon Nanofiber–Cobalt Oxide Composites. *Electrochim. Acta* **2008**, *53*, 7326–7330.
17. Wang, Y.; Zhang, H. J.; Lu, L.; Stubbs, L. P.; Wong, C. C; Lin, J. Y. Designed Functional Systems from Peapod-like Co@Carbon to Co_3O_4@Carbon Nanocomposites. *ACS Nano* **2010**, *4*, 4753–4761.
18. Novoselov, K. S.; Geim, A. K.; Morozov, S. V.; Jiang, D.; Zhang, Y.; Dubonos, S. V.; Grigorieva, I. V.; Firsov, A. A. Electric Field Effect in Atomically Thin Carbon Films. *Science* **2004**, *306*, 666–669.
19. Novoselov, K. S.; Jiang, D.; Schedin, F.; Booth, T. J.; Khotkevich, V. V.; Morozov, S. V.; Geim, A. K. Two-Dimensional Atomic Crystals. *Proc. Natl. Acad. Sci. U.S.A.* **2005**, *102*, 10451–10453.
20. Novoselov, K. S.; Geim, A. K.; Morozov, S. V.; Jiang, D.; Katsnelson, M. I.; Grigorieva, I. V.; Dubonos, S. V.; Firsov, A. A. Two-Dimensional Gas of Massless Dirac Fermions in Graphene. *Nature* **2005**, *438*, 197–200.
21. Geim, A. K. Graphene: Status and Prospects. *Science* **2009**, *324*, 1530–1534.
22. Zhou, G. M.; Wang, D. W.; Li, F.; Zhang, L. L.; Li, N.; Wu, Z.-S.; Wen, L.; Lu, G. Q.; Cheng, H. M. Graphene-Wrapped Fe_3O_4 Anode Material with Improved Reversible Capacity and Cyclic Stability for Lithium Ion Batteries. *Chem. Mater.* **2010**, *22*, 5306–5313.
23. Li, B. J.; Cao, H. Q.; Shao, J.; Qu, M. Z.; Warner, H. H. Superparamagnetic Fe_3O_4 Nanocrystals@Graphene Composites for Energy Storage Devices. *J. Mater. Chem.* **2011**, *21*, 5069–5075.
24. Wang, J. Z.; Zhong, C.; Wexler, D.; Idris, N. H.; Wang, Z. X.; Chen, L. Q.; Liu, H. K. Graphene-Encapsulated Fe_3O_4 Nanoparticles with 3D Laminated Structure as Superior Anode in Lithium Ion Batteries. *Chem.—Eur. J.* **2011**, *17*, 661–667.
25. Ji, L. W.; Tan, Z. K.; Kuykendall, T. R.; Aloni, S.; Xun, S.; Lin, E.; Battaglia, V.; Zhang, Y. G. Fe_3O_4 Nanoparticle-Integrated Graphene Sheets for High-Performance Half and Full Lithium Ion Cells. *Phys. Chem. Chem. Phys.* **2011**, *13*, 7170–7177.
26. Zhu, X. J.; Zhu, Y. W.; Murali, S.; Stoller, M. D.; Ruoff, R. S. Nanostructured Reduced Graphene Oxide/Fe_2O_3 Composite as a High-Performance Anode Material for Lithium Ion Batteries. *ACS Nano* **2011**, *5*, 3333–3338.
27. Wu, Z. S.; Ren, W. C.; Wen, L.; Gao, L. B.; Zhao, J. P.; Chen, Z. P.; Zhou, G. M.; Li, F.; Cheng, L. M. Graphene Anchored with Co_3O_4 Nanoparticles as Anode of Lithium Ion Batteries with Enhanced Reversible Capacity and Cyclic Performance. *ACS Nano* **2010**, *4*, 3187–3194.
28. Yang, S. B.; Feng, X. L.; Ivanovici, S.; Müllen, K. Fabrication of Graphene-Encapsulated Oxide Nanoparticles: Towards High-Performance Anode Materials for Lithium Storage. *Angew. Chem. Int. Ed.* **2010**, *49*, 1–5.
29. Li, B. J.; Cao, H. Q.; Shao, J.; Li, G. Q.; Qu, M. Z.; Yin, G. Co_3O_4@Graphene Composites as Anode Materials for High-Performance Lithium Ion Batteries. *Inorg. Chem.* **2011**, *50*, 1628–1632.
30. Chen, S. Q.; Wang, Y. Microwave-Assisted Synthesis of a Co_3O_4–Graphene Sheet-on-Sheet Nanocomposite as a Superior Anode Material for Li-Ion Batteries. *J. Mater. Chem.* **2010**, *20*, 9735–9739.
31. Kim, H.; Seo, D.-H.; Kim, S.-W.; Kim, J.; Kang, K. Highly Reversible Co_3O_4/Graphene Hybrid Anode for Lithium Rechargeable Batteries. *Carbon* **2011**, *49*, 326–332.
32. Wang, H. L.; Cui, L. F.; Yang, Y.; Casalongue, H. S.; Robinson, J. T.; Liang, Y. Y.; Cui, Y.; Dai, H. J. Mn_3O_4–Graphene Hybrid as a High-Capacity Anode Material for Lithium Ion Batteries. *J. Am. Chem. Soc.* **2010**, *132*, 13978–13980.
33. Zou, Y. Q.; Wang, Y. NiO Nanosheets Grown on Graphene Nanosheets as Superior Anode Materials for Li-Ion Batteries. *Nanoscale* **2011**, *3*, 2615–2620.
34. Wang, B.; Wu, X. L.; Shu, C. Y.; Guo, Y. G.; Wang, C. R. Synthesis of CuO/Graphene Nanocomposite as a High-Performance Anode Material for Lithium-Ion Batteries. *J. Mater. Chem.* **2010**, *20*, 10661–10664.
35. Xu, C.; Wang, X.; Yang, L. C.; Wu, Y. P. Fabrication of a Graphene–Cuprous Oxide Composite. *J. Solid State Chem.* **2009**, *182*, 2486–2490.
36. Wang, D. H.; Kou, R.; Choi, D. W.; Yang, Z. G.; Nie, Z. M.; Li, J.; Saraf, L. V.; Hu, D. H.; Zhang, J. G.; Graff, G. L.; *et al.* Ternary Self-Assembly of Ordered Metal Oxide-Graphene Nanocomposites for Electrochemical Energy Storage. *ACS Nano* **2010**, *4*, 1587–1595.
37. Paek, S.-M.; Yoo, E.; Honma, I. Enhanced Cyclic Performance and Lithium Storage Capacity of SnO_2/Graphene Nanoporous Electrodes with Three-Dimensionally Delaminated Flexible Structure. *Nano Lett.* **2009**, *9*, 72–75.
38. Zhang, L. S.; Jiang, L. Y.; Yan, H. J.; Wang, W. D.; Wang, W.; Song, W. G.; Guo, Y. G; Wan, L. J. Mono Dispersed SnO_2 Nanoparticles on Both Sides of Single Layer Graphene Sheets as Anode Materials in Li-Ion Batteries. *J. Mater. Chem.* **2010**, *20*, 5462–5467.
39. Wang, D. H.; Choi, D. W.; Li, J.; Yang, Z. G.; Nie, Z. M.; Kou, R.; Hu, D. H.; Wang, C. M.; Saraf, L. V.; Zhang, J. G.; *et al.* Self-Assembled TiO_2–Graphene Hybrid Nanostructures for Enhanced Li-Ion Insertion. *ACS Nano* **2009**, *3*, 907–914.
40. Qiu, Y. C.; Yan, K. Y.; Yang, S. H.; Jin, L. M.; Deng, H.; Li, W. S. Synthesis of Size-Tunable Anatase TiO_2 Nanospindles and Their Assembly into Anatase@Titanium Oxynitride/Titanium Nitride–Graphene Nanocomposites for Rechargeable Lithium Ion Batteries with High Cycling Performance. *ACS Nano* **2010**, *4*, 6515–6526.
41. Ding, S. J.; Chen, J. S.; Luan, D. Y.; Boey, F. Y. C.; Madhavi, S.; Lou, X. W. Graphene-Supported Anatase TiO_2 Nanosheets for Fast Lithium Storage. *Chem. Commun.* **2011**, *47*, 5780–5782.

42. Armand, M.; Tarascon, J.-M. Building Better Batteries. *Nature* **2008**, *45*, 652–657.
43. Ye, J. F.; Liu, W.; Cai, J. G.; Chen, S.; Zhao, X. W.; Zhou, H. H.; Qi., L. M. Nanoporous Anatase TiO_2 Mesocrystals: Additive-Free Synthesis, Remarkable Crystalline-Phase Stability, and Improved Lithium Insertion Behavior. *J. Am. Chem. Soc.* **2011**, *133*, 933–940.
44. Hu, Y. S.; Guo, Y. G.; Dominko, R.; Gaberscek, M.; Jamnik, J.; Maier, J. Improved Electrode Performance of Porous $LiFePO_4$ Using RuO_2 as an Oxidic Nanoscale Interconnect. *Adv. Mater.* **2007**, *19*, 1963–1966.
45. Choi, J.; Jin, J.; Jung, G. I.; Kim, J. M.; Kim, H. J.; Son, S. U. $SnSe_2$ Nanoplate−Graphene Composites as Anode Materials for Lithium Ion Batteries. *Chem. Commun.* **2011**, *47*, 5241–5243.
46. Yao, J.; Shen, X. P.; Wang, B.; Liu, H. K.; Wang, G. X. *In Situ* Chemical Synthesis of SnO_2-Graphene Nanocomposite as Anode Materials for Lithium-Ion Batteries. *Electrochem. Commun.* **2009**, *11*, 1849–1852.
47. Nam, K. T.; Kim, D. W.; Yoo, P. J.; Chiang, C. Y.; Meethong, N.; Hammond, P. T.; Chiang, Y. M.; Belcher, A. M. Virus-Enabled Synthesis and Assembly of Nanowires for Lithium Ion Battery Electrodes. *Science* **2006**, *312*, 885–888.
48. Yoo, E.; Kim, J.; Hosono, E.; Zhou, H. S.; Kudo, T.; Honma, I. Large Reversible Li Storage of Graphene Nanosheet Families for Use in Rechargeable Lithium Ion Batteries. *Nano Lett.* **2008**, *8*, 2277–2282.
49. Pan, D. Y.; Wang, S.; Zhao, B.; Wu, M. H.; Zhang, H. J.; Wang, Y.; Jiao, Z. Li Storage Properties of Disordered Graphene Nanosheets. *Chem. Mater.* **2009**, *21*, 3136–3142.
50. Wang, G. X.; Wang, B.; Wang, X. L.; Park, J.; Dou, S. X.; Ahn, H.; Kim, K. Sn/Graphene Nanocomposite with 3D Architecture for Enhanced Reversible Lithium Storage in Lithium Ion Batteries. *J. Mater. Chem.* **2009**, *19*, 8378–8384.
51. Laruelle, S.; Grugeon, S.; Poizot, P.; Dolle, M.; Dupont, L.; Tarascon, J. M. On the Origin of the Extra Electrochemical Capacity Displayed by MO/Li Cells at Low Potential. *J. Electrochem. Soc.* **2002**, *149*, A627–A634.
52. Wei, L.; Tang, D. M.; He, Y. B.; You, C. H.; Shi, Z. Q.; Chen, X. C.; Chen, C. M.; Hou, P. X.; Liu, C.; Yang, Q. H. Low-Temperature Exfoliated Graphenes: Vacuum-Promoted Exfoliation and Electrochemical Energy Storage. *ACS Nano* **2009**, *3*, 3730–3736.